ISSN 1063-7834, Physics of the Solid State, 2020, Vol. 62, No. 11, pp. 2116–2121. © Pleiades Publishing, Ltd., 2020.
Russian Text © The Author(s), 2020, published in Fizika Tverdogo Tela, 2020, Vol. 62, No. 11, pp. 1882–1887.

IMPURITY CENTERS

Paramagnetic V^{2+} Centers in Yttrium–Aluminum Garnet

V. A. Vazhenin[a], *, A. P. Potapov[a], G. R. Asatryan[b], and M. Yu. Artyomov[a]

[a] *Ural Federal University, Institute of Natural Sciences and Mathematics, Yekaterinburg, Russia*

[b] *Ioffe Institute, St. Petersburg, Russia*

**e-mail: Vladimir.Vazhenin@urfu.ru*

Received June 16, 2020; revised June 16, 2020; accepted June 24, 2020

Abstract—Investigation of the EPR spectrum of $Y_3Al_5O_{12}$:V crystals have made it possible to determine the parameters of the fine and hyperfine structures of trigonal V^{2+} centers. The existence of V^{2+} triclinic centers that arise as a result of association of V^{2+} sites with defects that lower the symmetry is established.

Keywords: garnet, impurity ions, paramagnetic resonance

DOI: 10.1134/S1063783420110372

1. INTRODUCTION

Crystals of yttrium–aluminum garnet $Y_3Al_5O_{12}$ (YAG) doped with V^{3+} ions are extensively used in laser technology, in particular, as passive shutters for near-infrared lasers and composite laser components for solid-state lasers. The phototropic properties of these crystals are determined by the energy structure and relaxation characteristics of the V^{3+} ions, which replaced Al^{3+} and are in a tetrahedral coordination environment of oxygen atoms (point symmetry group S_4).

Vanadium ions in charge state V^{2+}, which substituted octahedral Al^{3+} positions with the C_{3i} symmetry in YAG, were discovered in [1, 2]. The authors of [1] observed X-band ESR signals of four magnetically nonequivalent V^{2+} centers with well-resolved hyperfine structure (HFS) in orientations $\mathbf{B} \parallel C_3$, C_4, and C_2 in the (**B** is the magnetic field induction) and interpreted them qualitatively without giving the values of the fine and hyperfine structure parameters.

In [2], the ESR spectra of YAG:V^{2+} in the frequency ranges of the X and Q bands, as well as in the frequency range of 22–70 GHz on a tunable spectrometer were studied. The values of the *g*-factor, zero-field splitting (ZFS), and parameters of hyperfine interaction (HFI) of trigonal V^{2+} centers were determined. The observed asymmetry of ESR lines of transition $-1/2 \leftrightarrow 1/2$ at $\mathbf{B} \parallel C_3$ was explained by the scatter of the rhombic parameter near its zero value. The origin of the rhombic distortion was not discussed [2].

In this study, the symmetry and structure of paramagnetic centers V^{2+} in yttrium–aluminum garnet crystals are investigated.

2. PREPARATION OF SAMPLES AND MEASUREMENT TECHNIQUES

The YAG:V^{2+} single crystals were grown at the Institute for Physical Research, Academy of Sciences of Armenian SSR (Ashtarak), by the method of vertical directional crystallization from the melt in molybdenum containers. In order to obtain V^{2+} ions embedded in the crystal, additional tetravalent impurities in the form of SiO_2 were introduced into the melt. The concentration of vanadium ions in the batch mixture was 0.03 at %.

The EPR spectra were recorded on an EMX Plus Bruker X-band spectrometer at room temperature in magnetic fields of up to 1.5 T. The samples were placed in a fluoroplastic barrel fixed on the rod of a standard uniaxial automatic goniometer, which enables the rotation of the crystal in the vertical plane. Thus, it was possible to obtain any orientation of the magnetic field in the sample.

3. RESULTS

As in [1, 2], four magnetically nonequivalent V^{2+} centers (electron spin $S = 3/2$) were observed in the EPR spectrum of the studied samples, the principal *Z* axes of which coincide with the trigonal crystal axes. The eight-component hyperfine structure of the HFS of electronic transitions arises from the interaction with ^{51}V nuclei (nuclear spin $I = 7/2$, natural abundance 99.76%). In a cubic YAG crystal (space group Ia3d (O_h^{10})), Al^{3+} ions occupy eight octahedral (local symmetry C_{3i}) and six tetrahedral (symmetry group S_4) positions [3]. The magnetic multiplicities for centers with spin $S = 3/2$ in these positions will be 4 for the octahedron and 3 for the tetrahedron. The Y^{3+} ions are

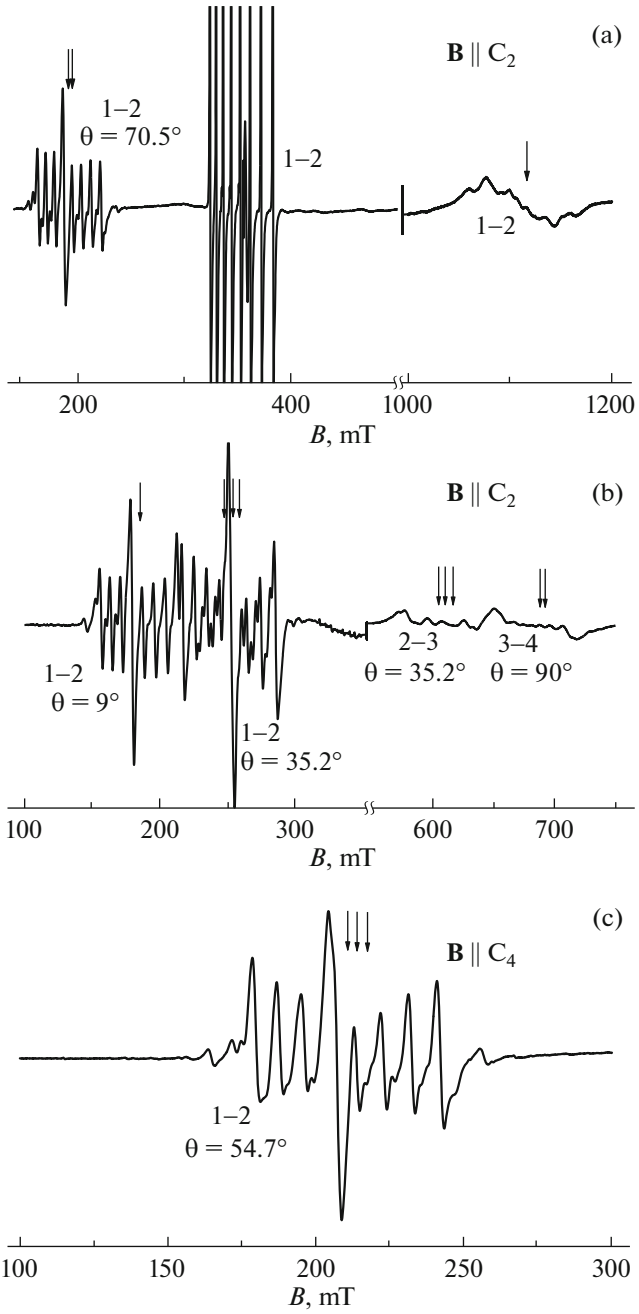

Fig. 1. EPR spectra (the first derivative of the absorption spectrum) of V^{2+} ions in orientations $\mathbf{B} \parallel C_3$, C_2, and C_4 at a frequency of 9847 MHz. The energy levels are numbered from bottom to top. The intensity of (a) the high-field transition at $\mathbf{B} \parallel C_3$ is increased by a factor of 5. The arrows show the positions of transitions of hypothetical triclinic centers with an even isotope.

located in oxygen cubes twisted around the C_4 axis and have the D_2 symmetry. Thus, it is apparent that vanadium ions replace Al^{3+} ions in octahedrally coordinated positions of the crystal lattice. Given that the charge states of the impurity ion and matrix aluminum

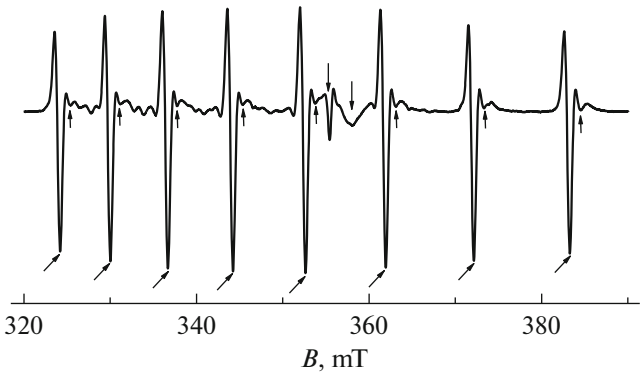

Fig. 2. EPR spectrum (second derivative of the absorption spectrum) of a YAG:V^{2+} crystal at $\mathbf{B} \parallel C_3$ at 9847 MHz. The lower inclined and vertical arrows show the positions of the transitions of the trigonal and triclinic V^{2+} centers, respectively. The upper arrows mark the signals of Cr^{3+} and Mo^{3+}.

are not identical, local charge compensation is possible.

Figures 1 and 2 show the EPR spectra of YAG:V^{2+} in orientations $\mathbf{B} \parallel C_3$, C_2, and C_4. The strongest signals inside the HFS of vanadium in all orientations of the magnetic field belong to the transitions of the trigonal Mo^{3+} center [4–6], which is a result of the interaction of the melt with the molybdenum container. Moreover, for the case of $\mathbf{B} \parallel C_3$ (Fig. 2), a weak signal of the trigonal Cr^{3+} center is observed near the signal of Mo^{3+} [7], which appeared in the crystal as an uncontrolled impurity. As in [2], the hyperfine components of the V^{2+} centers exhibit strong asymmetry (Fig. 2). The spectra show that transition $1 \leftrightarrow 2$ (corresponds to transition $-1/2 \leftrightarrow +1/2$ in the notation given in [1, 2]) of the hypothetical even isotope of the vanadium ion, which is detected near $g \approx 2$ at $\mathbf{B} \parallel C_3$, moves to the region of $g_{\text{eff}} \approx 4$ at $\mathbf{B} \perp C_3$. This behavior of the g-factor indicates that the center under study has electron spin $S = 3/2$ and the approximation of weak magnetic field (microwave frequency $\nu <$ ZFS) is fulfilled for it (as well as for the Mo^{3+} center).

The spectrum of the trigonal V^{2+} center can be described by a spin Hamiltonian of the following form [8]:

$$H_{\text{sp}} = 1/3 b_{20} O_{20} + \beta(\mathbf{BgS}) + (\mathbf{SAI}) + 1/3 Q O_{20}(I) - g_n \beta_n (\mathbf{BI}), \quad (1)$$

where $\mathbf{g}$ is the g tensor, β is the Bohr magneton, O_{20} is the Stevens spin operator, b_{20} is the fine structure parameter, $\mathbf{I}$ and $O_{20}(I)$ are the Stevens nuclear spin operators, $\mathbf{A}$ is the hyperfine interaction tensor, Q is the quadrupole interaction parameter, g_n is the nuclear g-factor, and β_n is the nuclear magneton.

It should be noted that the problem of optimizing the parameters of Eq. (1) cannot be divided into stages of determining the fine and, subsequently, hyperfine constants because of the large value and apparent nonequidistance of the HFS (Fig. 2). In addition, the absence of transitions from the HFS of eight intense components that are attributed to intradublet transition 3–4 and interdoublet transition 2–3 in the experimental spectrum predetermines a large error in the b_{20} parameter, since the positions of the HFS components of intradublet transition 1–2 determine the ZFS value only indirectly.

The use of the positions of the most intense HFS components of five electronic transitions (two transitions at $\mathbf{B} \parallel C_3$, two transitions at $\mathbf{B} \parallel C_2$, and one transition at $\mathbf{B} \parallel C_4$) and the orientational behavior of the HFS components of transition $1 \leftrightarrow 2$ in the range of polar angles $\theta = 0–19°$, as well as the diagonalizations of the 32-order energy matrix ($(2S+1)(2I+1)$), in the fitting procedure led to the following values of the parameters of Eq. (1) in coordinate system $\mathbf{Z} \parallel C_3$ over sixty six experimental points with a standard deviation of $F = 17$ MHz:

$$g_{\parallel} = 1.985, \quad g_{\perp} = 1.975, \quad |b_{20}| = 10\,545 \text{ MHz},$$
$$A_z = 234 \text{ MHz}, \quad A_{\perp} = 226 \text{ MHz}.$$

The small number of experimental points is due to the difficulty of assigning the HFS components to the corresponding electronic–nuclear energy sublevels in the polar angular dependence near C_3. At small angles (up to $\theta = 7°$), the high-field components fall into the region of intersection of electronic states $+1/2$ and $-3/2$; at large angles, the mid-field components are split into a large number of components comparable in intensity, due to the appearance of forbidden transitions in the HFS (electronic transitions with a change in the projection of the nuclear spin). Comparison of the obtained values with the published results [1, 2] shows a substantial difference in the values of some constants. Moreover, it should be born in mind that the b_{20} and ZFS values are confused in [1].

4. DISCUSSION

Figure 3 shows the electronic energy levels and only the observable transitions (Figs. 1 and 2) of the V^{2+} centers in orientations $\mathbf{B} \parallel C_3$, C_2, which are calculated using the parameters of Eq. (2), but excluding the HFS. Most electronic–nuclear states in the region of the intersection of levels $-3/2$ and $+1/2$ are repulsed due to hyperfine interaction, which can lead to distortion of the hyperfine structure. According to the calculations, the intensities of transitions 3–4 in orientations $\theta = 0°$, $\theta = 70.5°$, and $\theta = 90°$ are extremely low and, as a result, their signals are not observed (Fig. 1).

The result of calculation with the above parameters of the HFS of transitions of V^{2+} in orientations $\mathbf{B} \parallel C_3$, C_4, and C_2 shows that there should be doublets of weaker signals between the intense components due to forbidden transitions. These doublets have the strongest intensity comparable with the intensity of the eight main HFS components at $\mathbf{B} \perp C_2$ (for $\theta = 35.26°$). The experimental and calculated HFSes of this transition are shown in Fig. 4. Unfortunately, the signal of the trigonal center of Mo^{3+} is superimposed on the central part of the structure, but the correlation in the intensities and positions of the doublets in the experimental and calculated spectra is clearly visible though. Reliable identification of forbidden transitions gives grounds for determining the quadrupole interaction parameter, and good match of the positions of all calculated and observed components in Fig. 4 indicates its small value relative to the A constant. With addition of the positions of forbidden transitions from orientation $\mathbf{B} \parallel C_2$ (Fig. 4) and addition-

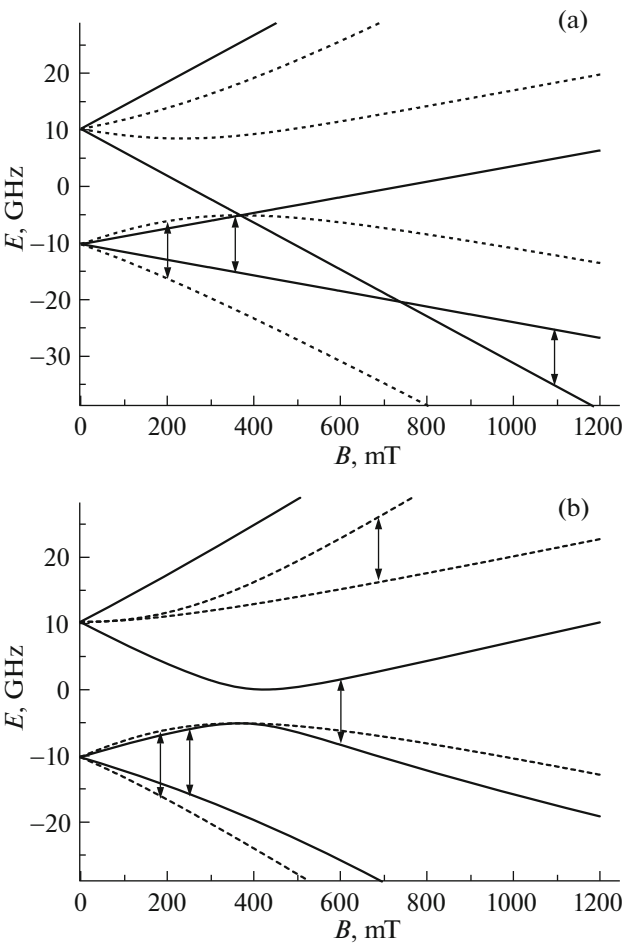

Fig. 3. Energy levels and the observed transitions of V^{2+} centers in the following orientations: (a) $\mathbf{B} \parallel C_3$, the solid curve corresponds to polar angle $\theta = 0°$, and the dashed line corresponds to $\theta = 70.5°$; (b) $\mathbf{B} \parallel C_2$, the solid curve corresponds to polar angle $\theta = 35.2°$, and the dashed line corresponds to $\theta = 90°$. The frequency is 9847 MHz.

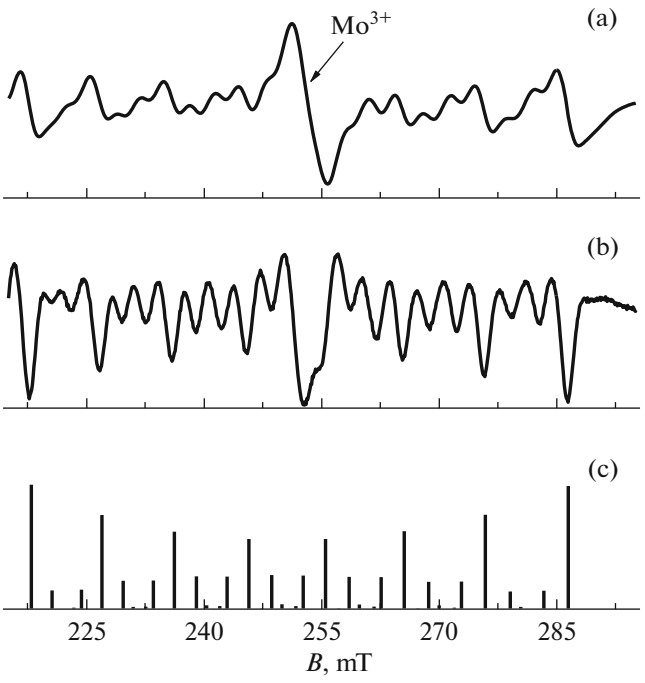

Fig. 4. Experimental and calculated HFSes of transition $1 \leftrightarrow 2$ at $\mathbf{B} \parallel C_2$: the (a) first and (b) second derivatives of the absorption spectrum, and (c) is the calculated spectrum.

ally identified (in the approximation of a small value of the quadrupole interaction parameter) HFS components from the polar angular dependence near C_3 to the fitting procedure, the following values were obtained for the parameters of Hamiltonian (1) over a hundred one experimental points with a standard deviation of $F = 18$ MHz:

$$g_{\parallel} = 1.985(5), \quad g_{\perp} = 1.975(5),$$
$$|b_{20}| = 10\,500(300)\ \text{MHz}, \quad A_z = 236(7)\ \text{MHz}, \quad (2)$$
$$A_{\perp} = 226(4)\ \text{MHz}, \quad Q = 3(5)\ \text{MHz}.$$

The handbook value of the nuclear g-factor was used in the calculations. The F value found is partially justified by the rather large width of the HFS components of V^{2+} ions in YAG (1.5–2.0 mT) and the difficulty in adjusting the required orientations of the magnetic field.

However, the result of calculation with parameters (3) obtained for the high-field interdoublet transition at $\mathbf{B} \parallel C_3$ gives eight identical HFS components (Fig. 5b), which completely disagree with the experimental result (Fig. 1a). A similar inconsistency between the results of calculation (Fig. 6b) and experiment is observed for transition $3 \leftrightarrow 4$ at $\theta = 90°$ (Fig. 1b). Furthermore, the intense octets of the HFS components used in the fitting procedure are accompanied by unidentified signals in the experiment (for example, see Fig. 1c). Finally, it is seen in Fig. 2 that eight intense HFS components of transition $1 \leftrightarrow 2$ ($-1/2 \leftrightarrow +1/2$) are accompanied by an octet of weak signals shifted by about 1 mT to high fields. Thus, it is obvious that the observed spectrum cannot be described assuming the existence of solely a trigonal center.

It can be assumed that the crystal contains, along with the trigonal V^{2+} center (C_{3i}), triclinic centers that arise as a result of either local charge compensation (for example, due to the presence of silicon, see Section 2) or the effects of unusual substitutions (antisite defects) [9]. The nearest cationic coordination spheres formed by Y^{3+}, Al_{oct}, and Al_{tetr} ions around the V^{2+} ions localized in the position of octahedral aluminum are octahedra distorted along the C_3 axis. Obviously, only one of the nearest cationic sites of these octahedra is substituted at a low concentration of defects (both antisite and silicon).

Typically, silicon (ionic radius 0.4 Å) forms covalently bound complexes $(SiO_4)^{4-}$ in oxide crystals, in which silicon is surrounded by an oxygen tetrahedron. Therefore, silicon in garnet must be in place of Al_{tetr}. The association of V^{2+} with such defects gives rise to six identical, but differently oriented centers with local symmetry C_1. Since three centers among the indicated six centers are connected by the inversion operation with three others, only three magnetically nonequivalent signals will be observed in the ESR spectra. Since the concentration of trigonal centers is much higher than the concentration of dimeric centers, it can be stated that the charge of vanadium centers is mainly compensated nonlocally.

If it is possible to rearrange the matrix ions [9] as a result of association of V^{2+} ions with defects $Y^{3+} \rightarrow Al_{oct}$ and $Al^{3+} \rightarrow Y^{3+}$, then two physically nonequivalent dimeric centers are also possible. Consequently, six more magnetically nonequivalent spectra could be expected in the experiment. However, ab initio calculations within the density functional theory method [10, 11] show that the Y_{Al} substitution of octahedral aluminum sites with yttrium ions is the most favorable mechanism among all possible mechanisms for the arrangement of excess yttrium cations in the YAG structure. Thus, the presence of antisite defects of the $Y^{3+} \rightarrow Al_{oct}$ type in the coordination environment of V^{2+} ions is an apparent reason for the appearance of triclinic centers.

To describe triclinic centers, Hamiltonian (1) must be supplemented with terms of the following form:

$$b_{21}O_{21} + b_{22}O_{22}, \quad (3)$$

where O_{2m} are the Stevens cosine operators [8].

The observed shift of the triclinic octet relative to the trigonal one (Fig. 2) can be explained by the influence of parameters $|b_{21}| \approx 2500$ MHz (downfield shift) and $|b_{22}| \approx 250$ MHz (upfield shift). Small variations of

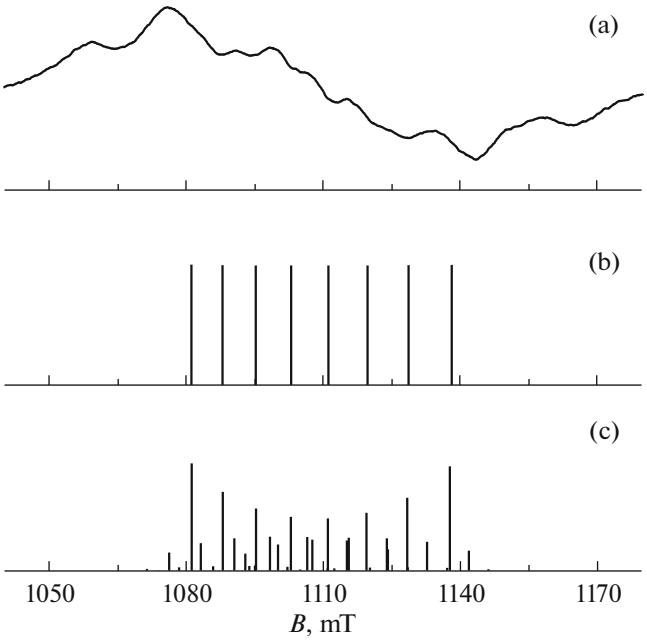

Fig. 5. Experimental and calculated shapes of the HFS of transition $1 \leftrightarrow 2$ ($-3/2 \leftrightarrow -1/2$) at $\mathbf{B} \parallel C_3$: (a) experiment; (b) calculation with $b_{20} = 10500$ MHz and $b_{21} = 0$; (c) calculation with $b_{20} = 10500$ MHz and $b_{21} = 2500$ MHz.

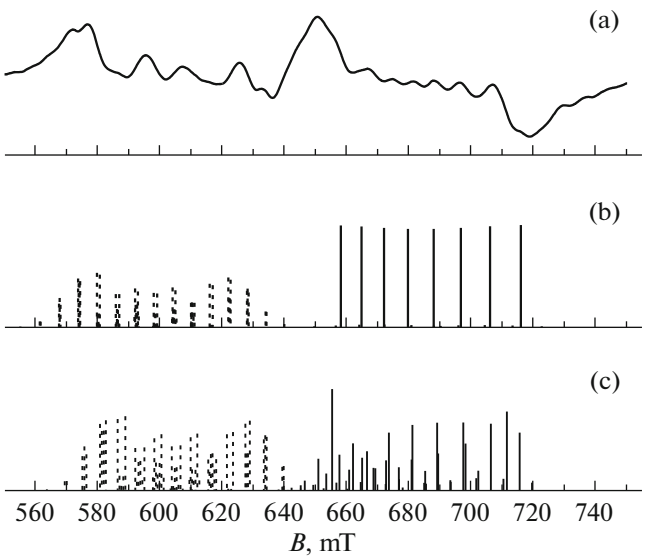

Fig. 6. Experimental and calculated shapes of the HFS of transition $2 \leftrightarrow 3$ at $\theta = 35.2°$ and transition $3 \leftrightarrow 4$ at $\theta = 90°$ (see Fig. 1b): (a) experiment; (b) calculation with $b_{20} = 10500$ MHz and $b_{21} = 0$; (c) calculation with $b_{20} = 10500$ MHz and $b_{21} = 2500$ MHz.

these parameters give rise to an experimental difference in the positions of two eight-component spectra (Fig. 2).

The appearance of the b_{22} term with the indicated value in Eq. (1) barely has an effect on the shape of the HFSes of high-field transitions at $\mathbf{B} \parallel C_3$, C_2; a substantial effect of the b_{21} parameter on the shape of these transitions is shown in Figs. 5c and 6c. As can be seen, the change in the intensity of the main HFS components and the appearance of a large number of forbidden electronic–nuclear transitions (see Figs. 5c and 6c) makes the calculated spectrum qualitatively close to the experimental one. According to the calculation results, satellite lines also appear in the eight hyperfine components of the transitions (at $\mathbf{B} \parallel C_3$, C_2, and C_4) used in the optimization procedure.

These calculations did not take into account the existence of spectra from two more triclinic centers rotated at angles $\varphi = \pm 2\pi/3$. To illustrate the contribution of this effect, the arrows in Fig. 1 show the positions of the transitions of three triclinic centers of the hypothetical even isotope of the vanadium ion with $|b_{21}| \approx 2500$ MHz.

Thus, the assumption of the existence of a V^{2+} triclinic center with approximate (estimated) parameters of the fine structure makes it possible to qualitatively explain the experimental spectrum in all orientations of the magnetic field. The existence of other triclinic centers (with lower values of b_{21} and b_{22}) is supported by the observed asymmetry of the line shape of the trigonal V^{2+} center (Fig. 2). The presence of several physically nonequivalent dimeric centers can substantially complicate the observed spectrum and reduce the degree of resolution of the hyperfine components.

To quantitatively describe these centers (with an arbitrary orientation of the X axis in the plane perpendicular to $Z \parallel C_3$), it is necessary to determine the values of all parameters of Eqs. (1) and (3), as well as the terms in form $c_{21}\Omega_{21} + c_{22}\Omega_{22}$, where Ω_{2m} are the Stevens sinusoidal operators and c_{2m} are the fine structure parameters [8]. To solve this problem, it is necessary to identify a sufficiently large number of electronic–nuclear transitions existing in the crystal of triclinic centers, which is not possible with the spectral resolution achieved in the experiments (Figs. 5c and 6c).

5. CONCLUSIONS

In the studied crystals of yttrium–aluminum garnet YAG:V, the EPR spectrum is a result of superposition of electronic–nuclear intense transitions of the trigonal V^{2+} center and weaker transitions of triclinic dimeric centers (perhaps of several types). Most likely, associates of V^{2+} with rearrangement defects of the $Y^{3+} \rightarrow Al_{oct}$ type or with the $(SiO_4)^{4-}$ complexes are the most common triclinic centers.

ACKNOWLEDGMENTS

We are grateful to A.V. Fokin for his assistance when performing calculations.

FUNDING

The part of the study performed by V.A. Vazhenin, A.P. Potapov, and M.Yu. Artemov is supported to the Ministry of Science and Education of the Russian Federation (topic no. FEUZ-2020-0054).

CONFLICT OF INTEREST

The authors declare that they have no conflicts of interest.

REFERENCES

1. I. I. Karpov, B. N. Grechushnikov, V. F. Koryagin, A. M. Kevorkov, and Fam Za Ngy, Sov. Phys. Dokl. **24**, 33 (1979).
2. G. V. Abagyan, G. R. Asatryan, A. A. Mirzakhanyan, L. A. Oganesyan, and A. K. Petrosyan, Sov. Phys. Solid State **31**, 339 (1989).
3. M. L. Meil'man and M. I. Samoilovich, *Introduction to EPR Spectroscopy of Activated Single Crystals* (Atomizdat, Moscow, 1977), p. 30 [in Russian].
4. Kh. S. Bagdasarov, V. V. Bershov, V. O. Martirosyan, and M. L. Meilman, Phys. Status Solidi B **46**, 745 (1971).
5. Kh. S. Bagdasarov, Yu. N. Dubrov, I. N. Marov, V. O. Martirosyan, and M. L. Meilman, Phys. Status Solidi B **56**, K65 (1973).
6. G. S. Shakurov, G. R. Asatryan, L. V. Mingalieva, A. G. Petrosyan, and K. L. Ovanesyan, Phys. Solid State **60**, 2046 (2018).
7. G. I. Vetrogon, V. I. Danilenko, V. Ya. Kabanchenko, V. V. Osiko, A. M. Prokhorov, A. N. Terent'evskii, and M. I. Timoshechkin, Sov. Phys. Solid State **22**, 1881 (1980).
8. S. A. Altshuler and B. M. Kozyrev, *Electron Paramagnetic Resonance in Compounds of Transition Elements* (Wiley, New York, 1974; Nauka, Moscow, 1972).
9. G. R. Asatryan, D. D. Kramushchenko, Yu. A. Uspenskaya, P. G. Baranov, and A. G. Petrosyan, Phys. Solid State **56**, 1150 (2014).
10. Bo Liu, Mu Gu, Xiaolin Liu, Shiming Huang, and Chen Ni, Appl. Phys. Lett. **94**, 121910 (2009).
11. A. B. Munoz-Garcia, E. Artacho, and L. Seijo, Phys. Rev. B **80**, 014105 (2009).

Translated by O. Kadkin